Supplementary Information to *Capillary deformations of bendable films*

R.D. Schroll, M. Adda-Bedia, J. Huang, N. Menon, T.P. Russsell, K.B. Toga, D. Vella, and B. Davidovitch

June 11, 2013

In the Letter, we discuss the solution of the Föppl–von Kármán equations that minimizes the free energy of a liquid drop on a thin elastic film, which is floating on a liquid bath. Herein, we provide the details of this calculation, as well as several additional results which could not be included in the main text. Additionally, we include some details on the measurements and the data analysis. The first section shows how we combine the many dimensional parameters into six relevant dimensionless parameters. In the second section, we write the free energy of our system, which consists of the elastic energy of the thin sheet as well as surface energies of all the interfaces. Notably, we demonstrate that the absolute surface energies of the sheet do not matter; only the difference in surface energies, which enters Young's law, is important. The configuration of the elastic sheet can be described by joining together two previously-found solutions. In section three, we review these solutions and discuss the matching conditions required to join them at the contact line. This matching leaves a single free parameter, which must be found by energy minimization, which we describe in the fourth section. The Letter shows solutions for an equilibrium contact angle of $\pi/2$; section five shows results where this contact angle varies. Finally, the sixth section presents an asymptotic analysis of our solution in the limit $\tilde{\gamma} \to 0$, which explains the scaling behavior seen in Fig. 2 of the Letter and Fig. S2 herein. The last section contains some experimental details concerning the measurements and image analysis.

SI.1 Dimensionless groups

There are ten dimensional parameters in play in the drop-on-sheet problem. There are three length scales: the size of the sheet R_o, the characteristic size of the drop, $\sqrt[3]{V}$, deduced from the volume, and the thickness of the sheet t. There is the stretching modulus of the sheet, $Y = Et$, and the body force of gravity ρg on the liquid. Finally there are a number of surface energies: γ between the drop and the air, γ_{sl} between the drop and the sheet, γ_{sv} between the sheet and the air, γ' between the bath and the air, and $\gamma_{sl'}$ between the bath and the sheet.

Since we can rescale the surface energies (*e.g.* by $Y = Et$) and lengths (*e.g.* by $\sqrt[3]{V}$), we are left with eight independent dimensionless parameters. However, we will show in the following section that the various surface energies of the sheet (γ_{sl}, γ_{sv}, and $\gamma_{sl'}$) do not appear independently; only the difference $\gamma_{sv} - \gamma_{sl}$ is important. Therefore, the five surface energies yield only three dimensionless groups:

$$\cos\vartheta_Y = (\gamma_{sv} - \gamma_{sl})/\gamma \tag{1}$$

$$\gamma'/\gamma \tag{2}$$

$$\tilde{\gamma} = \gamma/Y \ , \tag{3}$$

such that we are left with six independent dimensionless parameters, as stated in the main text.

Instead of $\sqrt[3]{V}$, we find it more convenient to use $R = (3V/2\pi)^{1/3}\sin\vartheta_Y(1 - \frac{3}{2}\cos\vartheta_Y + \frac{1}{2}\cos^3\vartheta_Y)^{-1/3}$, which is simply the contact radius of the drop on an undeformed substrate. An important dimensionless

group is the *bendability* parameter (ϵ^{-1}) [1], which measures the ratio between radial bending and tensile forces:

$$\epsilon^{-1} = \gamma R^2/B \ , \ , \tag{4}$$

where $B = Et^3/12(1-\nu^2)$ is the bending modulus and the Poisson ratio ν is another dimensionless parameter in this problem, but has little effect. We consider here a Hookean response of the sheet to the applied tension (*i.e.* local response described by linear material elasticity). This is valid if γ is sufficiently small compared to the stretching modulus Y. Therefore, we have $\tilde{\gamma} \ll 1$, and hence we neglect in our calculations quadratic terms (and higher orders) in $\tilde{\gamma}$. Note that for the conditions $\epsilon^{-1} \gg 1$ (high bendability) and $\tilde{\gamma} \ll 1$ (Hookean response) to be simultaneously satisfied, the sheet's thickness t must be in the range:

$$\ell_m \ll t \ll \ell_m^{1/3} R^{2/3} \ , \tag{5}$$

where $\ell_m = \gamma/E$. In our experiments ℓ_m is at molecular scale whereas R is approximately 1 mm, and the sheet's thickness t (which ranges from tens to hunderds of nm's) always satisfies the condition (5).

In addition to the four dimensionless groups in Eqs. (1-4), two other dimensionless parameters are associated with the *deformability* of the substrate:

$$\tilde{K} = \rho g R^2/\gamma \ , \tag{6}$$

and the ratio of the drop to sheet size is

$$\tilde{R} = R/R_o \tag{7}$$

In this work, we consider only the limit of a small drop on a large sheet, where the actual (small) values of $\tilde{K}$ and $\tilde{R}$ affect only small perturbations to the analysis. Therefore, the four relevant dimensionless parameters for our study are those given in (1–4).

SI.2 Energy

The equilibrium configuration is the one that minimizes the total energy of the system. We may write this energy schematically as

$$U = U_{\text{elastic}} + \gamma_{sl'} A_{\text{bath/sheet}} + \gamma_{sl} A_{\text{sheet/drop}} + \gamma_{sv} A_{\text{sheet/vapor}} + \gamma' A_{\text{bath}} + \gamma A_{\text{drop}} \ . \tag{8}$$

The term U_{elastic} contains, in general, both in-plane and bending elastic energies. The other five terms are surface energies, given by products of surface tensions and corresponding areas of the bottom of the sheet, the top of the sheet under the drop, the top of the sheet outside the drop, the exposed bath, and the drop surface, respectively. While these terms involve all five surface energies, we will show below that, by shifting our reference state, the first three surface energy terms can be combined into a term of the form

$$(\gamma_{sv} - \gamma_{sl}) A_{\text{sheet/vapor}} \ , \tag{9}$$

and a constant term that does not affect the shape. This observation underlies the above construction of the relevant dimensionless groups.

The elastic energy consists of bending energy and in-plane elastic energy, the ratio of which is $\sim \epsilon^{1/2}$. In the high-bendability regime we investigate, where $\epsilon \ll 1$, the bending energy is negligible compared to leading-order terms. (This is the conclusion of the *far-from-threshold* theory of wrinkling [1].) Thus, we may write the relevant portion of the elastic energy as

$$U_{\text{elastic}} = \int_{I+O} d^2\tilde{x} \ \left(\tfrac{1}{2}\lambda \tilde{\varepsilon}_{ii}^2 + \mu \tilde{\varepsilon}_{ij}^2\right) \tag{10}$$

The area I represents the area of the sheet beneath the drop ($\tilde{r} < \tilde{R}_i$; note that $\tilde{R}_i$ is not fixed), and O is the area outside of the drop ($\tilde{R}_i < \tilde{r} < \tilde{R}_o$). λ and μ are the Lamé coefficients. The $\tilde{x}$ coordinates are

material coordinates of the undeformed sheet. The strain tensor $\tilde{\varepsilon}_{ij} = \frac{1}{2}\left(\tilde{u}_{i,j} + \tilde{u}_{j,i} + \zeta_{,i}\zeta_{,j}\right)$, where $\tilde{u}_i$ is the in-plane displacement vector, ζ is the out-of-plane displacement, and $\cdot_{,i}$ indicates $\partial_i \cdot$. The tilde'd material coordinates are chosen such that there is no elastic stress in the sheet when $\tilde{u}_i = 0$; that is, they represent the rest configuration for a system with no surface energies.

Of course, our system does have surface energies, so a more natural set of coordinates would correspond to the rest configuration under those surface energies. Given the space-varying surface energy of the top of the sheet (due to the presence of the drop), we cannot easily account for all the surface energies. Instead, we introduce new material coordinates x that correspond to a rest configuration under surface energy of $\gamma_{sl'} + \gamma_{sl}$. This means that in the new coordinate system region I will have no separate surface energy term, while region O will have an effective surface energy of $\gamma_{sl'} + \gamma_{sv} - (\gamma_{sl'} + \gamma_{sl}) = \gamma\cos\vartheta_Y$. To see this, write the first four terms of Eq. (8):

$$\begin{aligned} &U_{\text{elastic}} + \gamma_{sl'}A_{\text{bath/sheet}} + \gamma_{sl}A_{\text{sheet/drop}} + \gamma_{sv}A_{\text{sheet/vapor}} \\ &\quad= \int_{I+O} d^2\tilde{x}\ \left(\tfrac{1}{2}\lambda\tilde{\varepsilon}_{ii}^2 + \mu\tilde{\varepsilon}_{ij}^2\right) + \int_{I+O} d^2\tilde{x}\,\gamma_{sl'}(1+\tilde{\varepsilon}_{ii}) + \int_{I} d^2\tilde{x}\,\gamma_{sl}(1+\tilde{\varepsilon}_{ii}) + \int_{O} d^2\tilde{x}\,\gamma_{sv}(1+\tilde{\varepsilon}_{ii}) \\ &\quad= \int_{I+O} d^2\tilde{x}\ \left[\tfrac{1}{2}\lambda\tilde{\varepsilon}_{ii}^2 + \mu\tilde{\varepsilon}_{ij}^2 + (\gamma_{sl'}+\gamma_{sl})\tilde{\varepsilon}_{ii}\right] + \int_{I+O} d^2\tilde{x}\,(\gamma_{sl'}+\gamma_{sl}) + \int_{O} d^2\tilde{x}\,(\gamma_{sv}-\gamma_{sl})(1+\tilde{\varepsilon}_{ii}) \end{aligned} \tag{11}$$

The second term is a constant, so we may drop it. By completing the square, we may rewrite the first term as

$$\int_{I+O} d^2\tilde{x}\ \left[\tfrac{1}{2}\lambda\tilde{\varepsilon}_{ii}^2 + \mu\tilde{\varepsilon}_{ij}^2 + (\gamma_{sl'}+\gamma_{sl})\tilde{\varepsilon}_{ii}\right] = \int_{I+O} d^2\tilde{x}\ \left(\tfrac{1}{2}\lambda\varepsilon_{ii}^2 + \mu\varepsilon_{ij}^2\right) + \int_{I+O} d^2\tilde{x}\,c \tag{12}$$

where $\varepsilon_{ij} \equiv \tilde{\varepsilon}_{ij} + \mathcal{E}\delta_{ij}$, with $\mathcal{E} \equiv \frac{1}{2}(\gamma_{sl'}+\gamma_{sl})/(\lambda+\mu)$, and c is a constant depending on the Lamé coefficients and the surface energies only (*i.e.* not on the strains). The second integral of the right-hand side may be dropped as a constant. The strain ε_{ij} is calculated from the new coordinates $x_i = \tilde{x}_i(1-\mathcal{E})$ and displacements $u_i = \tilde{u}_i + \mathcal{E}\tilde{x}_i$. [The opposite signs in x_i and u_i come from requiring the Cartesian coordinates of a point to be the same in either material coordinate system: $x_i + u_i(x) = \tilde{x}_i + \tilde{u}_i(\tilde{x})$.] Since $\mathcal{E} \ll 1$, we retain only terms of $\mathcal{O}(\mathcal{E})$ when working out $\tilde{\varepsilon}_{ii} = \varepsilon_{ii} - 2\mathcal{E}$ and $d^2\tilde{x} = d^2x\,(1+2\mathcal{E})$. (This is consistent with the assumed Hookean response at $\tilde{\gamma} \ll 1$). Since the elastic term in Eq. (12) will prove to be small, we may take $d^2\tilde{x} \approx d^2x$ on the right-hand side. The final term of Eq. (11) may therefore be written as

$$\begin{aligned} \int_O d^2x\,(1+2\mathcal{E})(\gamma_{sv}-\gamma_{sl})(1+\varepsilon_{ii}-2\mathcal{E}) &= \gamma\cos\vartheta_Y \int_O d^2x\,(1+\varepsilon_{ii}) \\ &= \gamma\cos\vartheta_Y\left(\pi(R_o^2 - R_i^2) + \int_O d^2x\,\varepsilon_{ii}\right) \end{aligned} \tag{13}$$

where we have used the definition of the Young angle, Eq. (1). The term proportional to R_o^2 is a constant and is dropped. Thus, we are left with

$$\begin{aligned} &U_{\text{elastic}} + \gamma_{sl'}A_{\text{bath/sheet}} + \gamma_{sl}A_{\text{sheet/drop}} + \gamma_{sv}A_{\text{sheet/vapor}} \\ &\qquad= \int_{I+O} d^2\tilde{x}\ \left(\tfrac{1}{2}\lambda\varepsilon_{ii}^2 + \mu\varepsilon_{ij}^2\right) - \pi\gamma\cos\vartheta_Y R_i^2 + \gamma\cos\vartheta_Y\int_O d^2x\,\varepsilon_{ii} + \text{constants}\ , \end{aligned} \tag{14}$$

demonstrating that the individual surface energies of the sheet do not matter, except through the parameter ϑ_Y.

The fifth term of (8) depends on A_{bath}, the exposed area of the bath on which the film is floating. We may write this area as some total area, A_{total}, less the area covered by the sheet:

$$A_{\text{bath}} = A_{\text{total}} - \int_{I+O} d^2x\,(1+u_{i,i}) = A_{\text{total}} - \int_{I+O} d^2x\ - 2\pi R_o u_r(R_o). \tag{15}$$

We have chosen to write the area integral in terms of the x coordinates; we could have equally well written it in terms of the $\tilde{x}$ coordinates and then transformed to get the same answer. As the first two terms are constant, the only term relevant to the energy is $-2\pi\gamma' R_o u_r(R_o)$.

The final term of (8) contains A_{drop}, the surface area of the drop, which takes the form of a section of a sphere with radius D down to colatitude ϑ. Therefore, it has surface area $A_{\text{drop}} = 2\pi D^2(1-\cos\vartheta)$. The radius of the cross-section at colatitude ϑ, where the drop meets the sheet, is $D\sin\vartheta$. By definition, this point is at material coordinate R_i, so the real-space radii must be equal: $D\sin\vartheta = R_i + u_r(R_i)$. Thus, we can work out the surface area

$$A_{\text{drop}} = 2\pi\left(\frac{R_i+u_r(R_i)}{\sin\vartheta}\right)^2(1-\cos\vartheta) \approx 2\pi R_i^2\frac{1-\cos\vartheta}{\sin^2\vartheta}\left(1+2\frac{u_r(R_i)}{R_i}\right) \tag{16}$$

where we include only terms that are first order in u_r.

Thus, the energy up to constant terms is

$$U = \int_{I+O} d^2x\ \left(\tfrac{1}{2}\lambda\varepsilon_{ii}^2+\mu\varepsilon_{ij}^2\right) - \pi\gamma\cos\vartheta_Y R_i^2 + \gamma\cos\vartheta_Y\int_O d^2x\,\varepsilon_{ii} \\ - 2\pi\gamma' R_o u_r(R_o) + 2\pi\gamma R_i^2\frac{1-\cos\vartheta}{\sin^2\vartheta}\left(1+2\frac{u_r(R_i)}{R_i}\right) \tag{17}$$

As we asserted above, this energy depends on the surface energies only through γ, γ', and ϑ_Y. We minimize this energy as follows: We fix R_i and find the configuration that minimizes the energy under that constraint. Under this "virtual" restriction, we can use existing solutions for the strain fields that will be discussed below. Then, we search (numerically) for the R_i that minimizes the energy amongst these solutions [1].

SI.3 Elastic Solutions

With R_i fixed, the configurations of the elastic sheet in regions I and O may be solved for separately, subject only to matching boundary conditions at $r = R_i$. In fact, both regions resemble previously-solved problems: Region I, an elastic disc subject to a constant pressure and a radial tension at its perimeter, resembles the drop-on-sheet problem [2]. Region O, an elastic annulus under differential tension, is the Lamé problem [1]. Both of these configurations have been recently solved in the far-from-threshold analysis. In this analysis, bending is ignored in the leading order and areas of compressive stress are replaced with wrinkled regions where the compressive stress vanishes. (Higher order terms that include bending may be used to describe details of the wrinkles, but we do not go so far in the current work.) Rather than reproduce the previous results, we will simply quote the previous results, noting a few slight differences in the current calculation.

Both regions are solved in the Föppl–von Kármán (FvK) framework, which describes a thin elastic sheet in the small-slopes limit. The sheet is described by a (two-dimensional) strain tensor field ε_{ij}, which is related to the stress tensor σ_{ij} by the standard linear elastic relations, and the out-of-place displacement field ζ. The FvK equations express equilibrium in the in- and out-of-plane directions:

$$\partial_i\sigma_{ij} = 0 \tag{18a}$$

$$B\Delta^2\zeta - \sigma_{ij}\partial_i\partial_j\zeta = P \tag{18b}$$

In the case of an axisymmetric problem with no shear, as is the base solution in both regions, the FvK equations reduce to

$$\partial_r(r\sigma_{rr}) - \sigma_{\theta\theta} = 0 \tag{19a}$$

$$B\Delta_r^2\zeta - \sigma_{rr}\partial_r^2\zeta - \sigma_{\theta\theta}r^{-1}\partial_r\zeta = P \tag{19b}$$

In region I, the sheet must satisfy both equations, with the pressure P being supplied by the Laplace pressure of the drop. In region O, however, there is no pressure acting on the sheet, so Eq. (19b) is satisfied by $\zeta = 0$ and only the in-plane stress equation (19a) need be solved.

[1] In principle, we could find the equilibrium configuration by minimizing directly over all strain fields ε_{ij} and contact radii R_i, with the constraint of constant volume of the drop. However, in the high bendability regime addressed in our study the two-step approach (fixing first R_i and only then minimizing the energy over those solutions) is more efficient.

SI.3.1 Region I

In the region $r < R_i$, we have an elastic sheet subject to a constant pressure, with a tension applied at R_i. This is analogous to the problem of a sheet floating on a liquid drop, discussed in [2]. The analysis there showed that in the high bendability regime ($\epsilon^{-1} \gg 1$), the solutions are governed by a single confinement parameter

$$\alpha \equiv \frac{P^2 Y R_i^2}{8\sigma_{rr}^{(I)}(R_i)^3} = \frac{Y \sin^2\vartheta}{2\gamma\beta^3} \tag{20}$$

where we define for convention

$$\beta(\alpha,\vartheta) \equiv \frac{\sigma_{rr}^{(I)}(R_i)}{\gamma} = \big(\frac{1}{2\tilde{\gamma}}\big)^{1/3}\big(\frac{\sin^2\vartheta}{\alpha}\big)^{1/3} \tag{21}$$

in order to simplify notations in the following equations. (Note that the setup of the drop-on-sheet experiment [2] corresponds to $\beta = 1$, but here it will depend on a matching condition with the outer solution.) The confinement parameter α governs the extent of the wrinkled region: For $\alpha < \alpha_{wr} \approx 5.16$, the sheet is in biaxial tension everywhere. For larger α, there exists a wrinkled region for $\sqrt[5]{\alpha_{wr}/\alpha}\, R_i < r < R_i$.

Three results from the previous work are needed. First, the radial displacement at R_i is

$$u_r(R_i) = -\frac{\beta\gamma R_i}{Y}\left(\frac{1}{5}\ln\frac{\alpha_{wr}}{\alpha} + \nu + \frac{1}{5}(\alpha - \alpha_{wr})\right) \tag{22}$$

Second, the total elastic energy is

$$\int_I d^2x\ \left(\tfrac{1}{2}\lambda\varepsilon_{ii}^2 + \mu\varepsilon_{ij}^2\right) = \frac{\pi\beta^2\gamma^2 R_i^2}{Y}\left(A - 2\nu B + \frac{1}{5}\ln\frac{\alpha}{\alpha_{wr}}\right) \tag{23}$$

where $A \approx 1.132$ and $B \approx 0.500$. Finally, we may use the profile to integrate the volume of the drop that lies below the level of the surface of the bath:

$$V_{\text{bulge}} = 2\pi R_i^3 \frac{\tilde{\gamma}\beta^2}{\sin\vartheta}\left(\alpha_{wr}C + \frac{1}{5}(\alpha - \alpha_{wr})\right) \tag{24}$$

with $C \approx 0.219$.

SI.3.2 Region O

The outer section of the sheet is an annulus under differential tension: $\tau\gamma'$ (to be determined by matching conditions) on the inner boundary and γ' on the outer boundary. This setup is known as the Lamé problem, and a FT solution is presented in [1]. Here, there is the complicating circumstance of a non-zero surface energy $\gamma\cos\vartheta_Y$ [see Eq. (17)]. The total stress in the sheet comes from both the elastic terms and surface energy terms:

$$\sigma_{ij} = \frac{\partial}{\partial\varepsilon_{ij}}\left(\tfrac{1}{2}\lambda\varepsilon_{ii}^2 + \mu\varepsilon_{ij}^2 + \gamma\cos\vartheta_Y\varepsilon_{ii}\right) = \sigma_{ij}^{\text{elas}} + \gamma\cos\vartheta_Y\delta_{ij} \tag{25}$$

where $\sigma_{ij}^{\text{elas}}$ is the stress purely from elastic components and is connected to the strain and displacement in the usual manner. This issue is discussed further in [3], where σ_{ij} is called the "effective stress" (noted as Σ_{ij} in [3]). The total stress must balance the applied forces on the boundaries, so we have $\sigma_{rr}(R_i) = \tau\gamma'$ and $\sigma_{rr}(R_o) = \gamma'$. This gives boundary conditions on the elastic stress of $\sigma_{rr}^{\text{elas}}(R_i) = \tau\gamma' - \gamma\cos\vartheta_Y$ and $\sigma_{rr}^{\text{elas}}(R_o) = \gamma' - \gamma\cos\vartheta_Y$. The FT condition of no compressive stress is $\sigma_{\theta\theta} > 0$, or $\sigma_{\theta\theta}^{\text{elas}} > -\gamma\cos\vartheta_Y$.

This change is effectively only an offset to the solution of [1]. As before, the confinement parameter is

$$\tau = \frac{\sigma_{rr}^{(O)}(R_i)}{\sigma_{rr}^{(O)}(R_o)} \tag{26}$$

In the limit that $\tilde{R} \ll 1$, wrinkles will appear for $R_i < r < \frac{\tau}{2} R_i$, assuming that $\tau > 2$. Three results follow straightforwardly:

$$u_r(R_i) = -\frac{\gamma R_i}{Y}\left[\tau\frac{\gamma'}{\gamma}\ln\frac{\tau}{2} + \cos\vartheta_Y + \nu\left(\tau\frac{\gamma'}{\gamma} - \cos\vartheta_Y\right)\right] \tag{27}$$

$$u_r(R_o) = \frac{R_o}{Y}\left(\gamma\cos\vartheta_Y(-1+\nu) + \gamma'\left[1-\nu-2\left(\frac{R_i}{R_o}\right)^2\left(\frac{\tau}{2}\right)^2 + \mathcal{O}\left(\frac{R_i}{R_o}\right)^4\right]\right) \tag{28}$$

$$\begin{aligned}\int_O d^2x\ \left(\tfrac{1}{2}\lambda\varepsilon_{ii}^2 + \mu\varepsilon_{ii}^2\right) = \frac{\pi R_o^2\gamma'^2}{Y}\left(1-\frac{\gamma\cos\vartheta_Y}{\gamma'}\right)^2(1-\nu) + \frac{\pi R_i^2\gamma^2}{Y}\Bigg[\left(\frac{\tau\gamma'}{\gamma}\right)^2\Bigg(\ln\frac{\tau}{2} - \frac{1}{2}\left(1+\frac{\gamma\cos\vartheta_Y}{\gamma'}\right) \\ + \nu\left[1-\frac{3}{2}\frac{\gamma\cos\vartheta_Y}{\gamma'} + \frac{1}{2}\left(\frac{\gamma\cos\vartheta_Y}{\gamma'}\right)^2\right]\Bigg) + 2(1+\nu)\frac{\tau\gamma'}{\gamma}\cos\vartheta_Y - (1+\nu)\cos^2\vartheta_Y + \mathcal{O}\left(\frac{R_i}{R_o}\right)^2\Bigg]\end{aligned} \tag{29}$$

Finally, we need to calculate the surface energy term

$$\begin{aligned}\gamma\cos\vartheta_Y\int_O d^2x\,\varepsilon_{ii} &= 2\pi\gamma\cos\vartheta_Y\int_{R_i}^{R_o} dr\ \left[\partial_r(ru_r) + \frac{1}{2}\left((\partial_r\zeta)^2 + \frac{1}{r^2}(\partial_\theta\zeta)^2\right)\right] \\ &= 2\pi\gamma\cos\vartheta_Y\left[R_o u_r(R_o) - R_i u_r(R_i) + \frac{1}{2}\int_{R_i}^{\frac{\tau}{2}R_i} dr\ \left(f'^2 + \frac{m^2}{r^2}f^2\right)\right]\end{aligned} \tag{30}$$

where in the last step, we have assumed a wrinkle profile of the form $\zeta(r,\theta) = f(r)\cos m\theta$. One result from [1] is that $f \sim \epsilon^{1/4}$ and $m \sim \epsilon^{-1/4}$. Thus, we may drop the f' term in the high-bendability limit, but the product mf remains finite. This product is given by the "slaving" condition [Eq. (3) of [4]]: $m^2f^2 = 4R_i\gamma'\tau r\ln(\tau R_i/2r)/Y$. We find

$$\gamma\cos\vartheta_Y\int_O d^2x\,\varepsilon_{ii} = 2\pi\gamma\cos\vartheta_Y\left[R_o u_r(R_o) - R_i u_r(R_i) + 2R_i^2\frac{\tau\gamma'}{Y}\left(\frac{\tau}{2} - \ln\frac{\tau}{2} - 1 + 2\nu\right)\right] \tag{31}$$

SI.3.3 Matching Conditions

The setup presented so far has five undetermined parameters: α, τ, ϑ, ϕ, and R_i, that characterize the geometry and force balance at the contact line (see Fig. S1). In this section we explain how four of these five unknowns are determined. (This expands the discussion in the paragraph around Eqs. (9-10) of the main text). The remaining free parameter will be set by an energy minimization scheme, discussed in the next section.

Geometry: Considering a fixed value of the angle ϑ, the contact radius R_i is determined from volume conservation of the liquid drop. If the substrate did not deform and the contact angle remained ϑ_Y, the contact radius R_i would be R, by definition. Since neither of these happens for a finite-stiffness sheet, we must guarantee volume conservation by allowing R_i to change. Let us recall that the control paramater R is defined in terms of the volume of the drop and the Young angle ϑ_Y:

$$V = \frac{2\pi}{3}R^3\frac{1-\frac{3}{2}\cos\vartheta_Y + \frac{1}{2}\cos^3\vartheta_Y}{\sin^3\vartheta_Y} \tag{32}$$

The drop's volume consists of two components: the volume inside the drop above the plane of the bath, V_{above}, and the volume of the bulge of the sheet below the level of the bath, V_{bulge}, Eq. (24). The former term may be calculated simply from geometry:

$$V_{\text{above}} = \frac{2\pi}{3}D^3\left(1-\tfrac{3}{2}\cos\vartheta + \tfrac{1}{2}\cos^3\vartheta\right) = \frac{2\pi}{3}\left[R_i + u_r(R_i)\right]^3\frac{1-\frac{3}{2}\cos\vartheta + \frac{1}{2}\cos^3\vartheta}{\sin^3\vartheta} \tag{33}$$

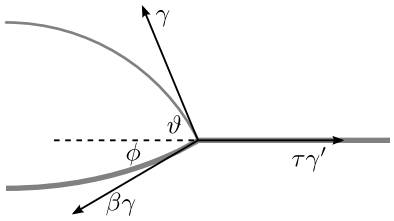

Figure S1: Geometry and force balance at the contact line at $r = R_i$. This figure is the same as Fig. 1b in the main text, with $\beta\gamma \equiv \sigma_{rr}^{(I)}(R_i)$ and $\tau\gamma' \equiv \sigma_{rr}^{(O)}(R_i)$.

As with the surface area calculation (16), we use $D\sin\vartheta = R_i + u_r(R_i)$ and expand up to first order in the displacement. Using Eq. (22) for $u_r(R_i)$ and combining Eqs. (24) and (33), we find the total volume to be

$$V = \frac{2\pi}{3}R_i^3\left[\frac{1-\frac{3}{2}\cos\vartheta+\frac{1}{2}\cos^3\vartheta}{\sin^3\vartheta}\left(1-3\tilde{\gamma}\beta\left[\frac{1}{5}\ln\frac{\alpha_{wr}}{\alpha}+\nu+\frac{1}{5}(\alpha-\alpha_{wr})\right]\right)\right.$$
$$\left.+\tilde{\gamma}\frac{3\beta^2}{\sin\vartheta}\left(\alpha_{wr}C+\frac{1}{5}(\alpha-\alpha_{wr})\right)\right] \quad (34)$$

Eq. (34) together with the definition (32) determine R_i as a function of the control parameters $R, \vartheta_Y, \tilde{\gamma}$, and the two unknowns α, ϑ. For completness, we note that the angle ϕ is readily evaluated from:

$$\zeta'(R_i) = \sin\phi \approx \phi \ , \quad (35)$$

but as we will see below, the angle ϕ is not actually required for the rest of the calculation.

Mechanics: At $r = R_i$ the sheet meets the surface of the drop, and we must have a force balance between the stresses in the sheet and the surface tension in the drop. This balance (see Fig. S1) may be divided into radial and vertical components:

$$\beta\gamma\cos\phi + \gamma\cos\vartheta = \tau\gamma' \quad (36a)$$
$$\beta\gamma\sin\phi + \gamma\sin\vartheta = 0 \quad (36b)$$

It is important to note that Eq. (36b) does not give rise to any other independent equation for the unknowns τ, ϑ, α, since it is automatically satisfied by the shape of the sheet below the drop. This reflects the fact that the entirety of the drop/sheet region must have no net vertical force, and is discussed further in [5].

We note that since $\sin\phi = \zeta'(R_i) \ll 1$ we can approximate $\cos\phi \approx 1$ and hence the angle ϕ is not required for our matching analysis. This is the same level of approximation used elsewhere in the Föppl–von Kármán equations. Eq. (36a) is exactly Eq. (9) of the main text.

Continuity: Eq. (10) of the main text reflects another condition that requires continuity of the sheet at $r = R_i$. This means that the radial displacements of the inner (22) and outer (27) sections must be equal.

Thus, the 4 equations which consist of Eqs. (34,35) and Eqs. (9,10) of the main text allow us to express the four unknowns R_i,ϕ,α and τ, as functions of the unknown angle ϑ [2]. For a given set of the control parameters, Eqs.(1-3), the solutions to the elastic problem are now governed by the single unknown ϑ.

SI.4 Energy

With Eqs. (22, 23, 28, 29), we have expressions for all of the terms in Eq. (17). There are several terms, proportional to R_o^2, which do not depend on R_i. As constants, these may be dropped. We also drop terms

[2]More precisely, the approximation $\phi \ll 1$ allowed us to eliminate the unknown ϕ, so that we are left with the 3 equations (Eq. (35) and Eqs. (9-10) of the main text) for the four unknowns: α, ϑ, R_i and τ.

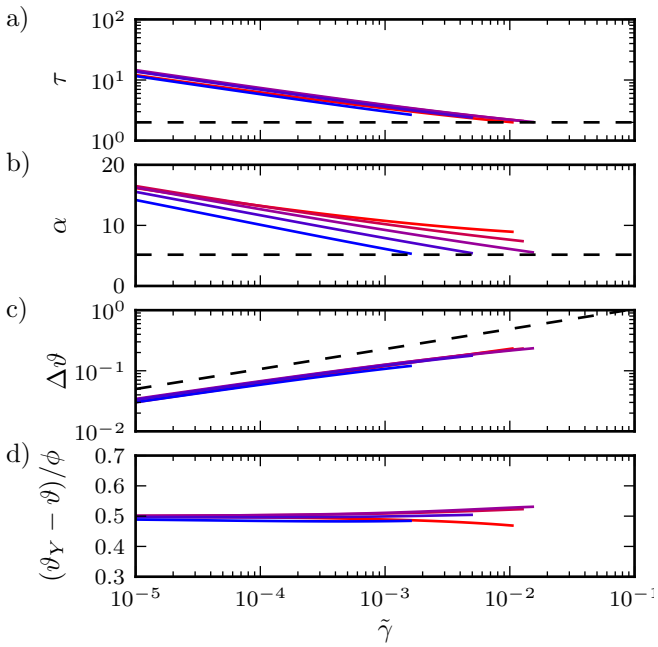

Figure S2: Results similar to Fig. 3 of the main text, but for fixed $\gamma'/\gamma = 1$ and $\vartheta_Y = \pi/4$ (red), $3\pi/8$, $\pi/2$, $5\pi/8$, and $3\pi/4$ (blue). Only the far-from-threshold solutions are plotted.

proportional to R_i^4/R_o^2 and higher, as they will not matter in the limit $R_o \gg R_i$. The remaining energy to be minimized is

$$U = \pi\gamma R_i^2 \left[2\frac{1-\cos\vartheta}{\sin^2\vartheta}\left(1 - 2\tilde{\gamma}\beta\left[\frac{1}{5}\ln\frac{\alpha_{wr}}{\alpha} + \nu + \frac{1}{5}(\alpha - \alpha_{wr})\right]\right) - \cos\vartheta_Y \right.$$
$$+ \tilde{\gamma}\left(\beta^2\left(A - 2\nu B + \frac{1}{5}\ln\frac{\alpha}{\alpha_{wr}}\right) + \cos^2\vartheta_Y(1-3\nu) + 2\cos\vartheta_Y\frac{\tau\gamma'}{\gamma}\left(\tau - 1 + 2\nu - \ln\frac{\tau}{2}\right)\right.$$
$$\left.\left. + \left(\frac{\tau\gamma'}{\gamma}\right)^2\left[\ln\frac{\tau}{2} + \frac{1}{2} - \frac{3}{2}\frac{\gamma\cos\vartheta_Y}{\gamma'} + \nu\left(1 - \frac{3}{2}\frac{\gamma\cos\vartheta_Y}{\gamma'} + \frac{1}{2}\left(\frac{\gamma\cos\vartheta_Y}{\gamma'}\right)^2\right)\right]\right)\right] \quad (37)$$

where R_i, α, β, τ are all expressed as functions of ϑ as was explained in the previous section. The minimization of Eq. (37) with respect to the angle ϑ reveals the equilibrium configuration.

SI.5 Results for $\vartheta_Y \neq \pi/2$

Figure 3 of the main text presents some results for a fixed $\vartheta_Y = \pi/2$ and several values of γ'/γ. These were chosen for display as the experiments could change γ' more easily than ϑ_Y. For completeness, we present in Fig. S2 results for a variety of ϑ_Y. Qualitatively, the results are similar. The values of τ and α are somewhat less coordinated in this case, which means that the inner and outer sections enter the FT regime at different points. As before, $\Delta\vartheta$ shows a scaling approaching $\tilde{\gamma}^{1/3}$. The ratio of the angles $\vartheta_Y - \vartheta$ and ϕ again approaches 0.5, but much more slowly than in the previous case.

SI.6 Asymptotic analysis of the limit $\tilde{\gamma} \to 0$

Figures 3 and S2 indicate some collapse of the data in the limit $\tilde{\gamma} \to 0$. We observe that $\alpha \sim \ln \tau$, and that both $\vartheta_Y - \vartheta$ and ϕ appear to scale approximately as $\tilde{\gamma}^{1/3}$, with a ratio that approaches 0.5. These behaviors may be understood by examining the drop-on-sheet solution in the limit $\tilde{\gamma} \to 0$. In this limit, we assume (and will show below) that $\tau \to \infty$, $\alpha \to \infty$, $\phi \to 0$, and $\vartheta \to \vartheta_Y$. We will use this last limit to replace ϑ with ϑ_Y to get the leading order behavior for other quantities. Only in the end, when we examine the energy, will we need to be careful about the difference between ϑ and ϑ_Y.

From the radial force balance at R_i (36a), we have

$$\beta \approx \tau \frac{\gamma'}{\gamma} - \cos\vartheta_Y \xrightarrow[\tau\to\infty]{} \tau \frac{\gamma'}{\gamma} \tag{38}$$

Note that, for $\vartheta_Y = \pi/2$, this last limit is an equality for all τ. Similarly, from Eq. (36b) we have

$$\phi \approx \zeta' \approx \frac{\sin\vartheta_Y}{\beta} \xrightarrow[\tau\to\infty]{} \frac{\gamma}{\gamma'} \frac{\sin\vartheta_Y}{\tau} \tag{39}$$

From the definition of α [Eq. (20)], we have

$$\alpha \approx \frac{\sin^2\vartheta_Y}{2\tilde{\gamma}\beta^3} \xrightarrow[\tau\to\infty]{} \left(\frac{\gamma}{\gamma'}\right)^3 \frac{\sin^2\vartheta_Y}{2\tilde{\gamma}\tau^3} \tag{40}$$

Note that these quantities depend only on τ, so we only need to apply displacement matching to understand the scaling.

In the FT analysis, the $u_r(R_i)$ matching is given by equating Eqs. (22) and (27). Using Eq. (38) for β, we see that the ν-dependent terms cancel on both sides, leaving us with

$$\left(\tau\frac{\gamma'}{\gamma} - \cos\vartheta_Y\right)\left(\frac{1}{5}\ln\frac{\alpha_{wr}}{\alpha} + \frac{1}{5}(\alpha - \alpha_{wr})\right) \approx \tau\frac{\gamma'}{\gamma}\ln\frac{\tau}{2} + \cos\vartheta_Y \tag{41}$$

In the limit $\tilde{\gamma} \to 0$, we will have $\alpha \gg \ln\alpha$ and $\tau \gg \cos\vartheta_Y$, so we further approximate this as

$$\frac{1}{5}\alpha \approx \ln\frac{\tau}{2} \tag{42}$$

(Note, again, that this approximation is significantly better for $\vartheta_Y = \pi/2$.) This explains the observation in Fig. 2a and 2b that $\alpha \sim \ln\tau$. Using the limit of Eq. (40), we get

$$\left(\frac{\gamma}{\gamma'}\right)^3 \frac{\sin^2\vartheta_Y}{\tilde{\gamma}} \approx 10\tau^3 \ln\frac{\tau}{2}\,, \tag{43}$$

a transcendental equation for τ. Plotting τ against the LHS of this equation, we do see a collapse of the data near the line predicted (see Fig. S3). To derive an expression for τ, we take the logarithms of both sides to find

$$3\ln\tau \approx 3\ln\frac{\gamma}{\gamma'} + 2\ln\sin\vartheta_Y - \ln\tilde{\gamma} - \ln 10 - \ln\ln\frac{\tau}{2} \approx -\ln\tilde{\gamma}\,. \tag{44}$$

The last approximation reflects the fact that all only $\tilde{\gamma}$ and τ are diverging and the double logarithm will do so very slowly. Using this expression for $\ln\tau$, we can find

$$\tau \approx \frac{\gamma}{\gamma'}\left(\frac{3}{10}\frac{\sin^2\vartheta_Y}{\tilde{\gamma}\ln\tilde{\gamma}}\right)^{1/3}\,. \tag{45}$$

Using Eq. (9) of the main text we now obtain the following approximation for the length of wrinkles:

$$L_O \approx \tfrac{1}{2}R_i\frac{\gamma}{\gamma'}\left(\frac{3}{10}\frac{\sin^2\vartheta_Y}{\tilde{\gamma}\ln\tilde{\gamma}}\right)^{1/3}\,. \tag{46}$$

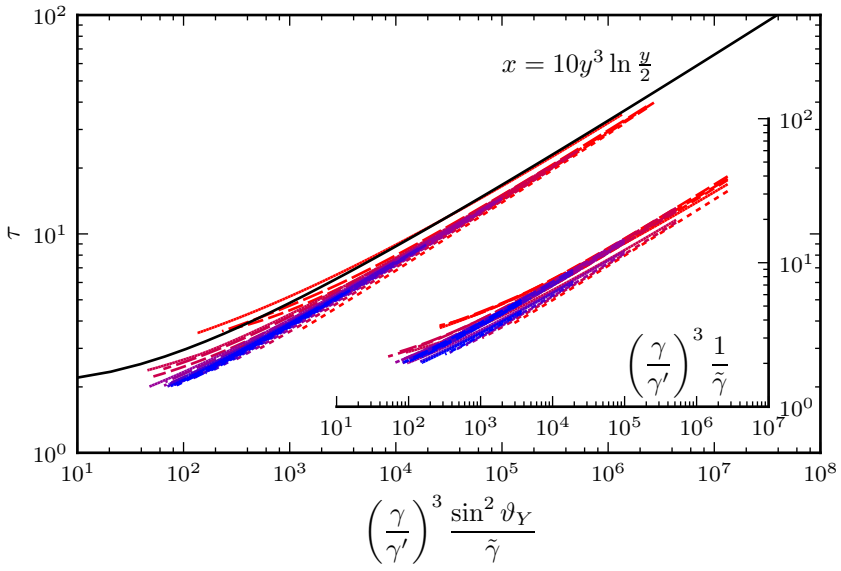

Figure S3: A test of the scaling predicted by Eq. (43). Twenty-five solutions with $\gamma'/\gamma = 0.33$ (red), 0.58, 1, 1.73, 3 (blue) and $\vartheta_Y = \pi/4$ (solid), $3\pi/8$, $\pi/2$, $5\pi/8$, $3\pi/4$ (dotted). There is an unexplained difference in the prefactor. Inset, the same data without the rescaling by $\sin^2 \vartheta_Y$, illustrating that this scaling does improve the collapse.

Plugging Eq. (45) into the limit of Eq. (39), we get

$$\phi \approx \left(-\tfrac{10}{3}\ \tilde{\gamma} \ln \tilde{\gamma}\ \sin \vartheta_Y\right)^{1/3} \quad . \tag{47}$$

This exponent and logarithm explain why the scaling of ϕ is observed to slowly approach $\tilde{\gamma}^{1/3}$.

The final part of the calculation is to find the contact angle by minimizing the energy, Eq. (37). In the leading-order terms, we must remember the difference between ϑ and ϑ_Y. In the $\mathcal{O}(\tilde{\gamma})$ terms, we may ignore this difference and use the approximations developed above. There are many different $\mathcal{O}(\tilde{\gamma})$ terms; the largest goes like $\tau^2 \ln \tau$. We will keep only these terms and ignore all others. As the next largest term is of order $\tau^2 \ln \ln \tau$, this is a rather poor approximation and will only be valid for very large τ. Thus, our approximation for the energy is

$$U \approx \pi \gamma R_i^2 \left[2\frac{1-\cos\vartheta}{\sin^2\vartheta} - \cos\vartheta_Y + \tilde{\gamma}\left(\frac{\tau\gamma'}{\gamma}\right)^2 \ln\frac{\tau}{2}\right] \tag{48}$$

Using the same level of approximation, we find the contact radius from Eq. (34)

$$R_i^{-3} \approx \frac{2\pi}{3V}\left[\frac{1-\frac{3}{2}\cos\vartheta+\frac{1}{2}\cos^3\vartheta}{\sin^3\vartheta} + \frac{3\tilde{\gamma}}{\sin\vartheta_Y}\left(\frac{\tau\gamma'}{\gamma}\right)^2 \ln\frac{\tau}{2}\right] \tag{49}$$

If we take $\partial U/\partial\vartheta = 0$ and grind through some algebra, we get

$$\cos\vartheta - \cos\vartheta_Y \approx 5\tilde{\gamma}\left(\frac{\tau\gamma'}{\gamma}\right)^2 \ln\frac{\tau}{2} \tag{50}$$

We may expand $\cos\vartheta \approx \cos\vartheta_Y - (\vartheta - \vartheta_Y)\sin\vartheta_Y$ and use Eq. (43) to substitute for $\tilde{\gamma}$ to find

$$\vartheta_Y - \vartheta \approx \frac{1}{2}\frac{\gamma}{\gamma'}\frac{\sin\vartheta_Y}{\tau} \approx \frac{1}{2}\phi \tag{51}$$

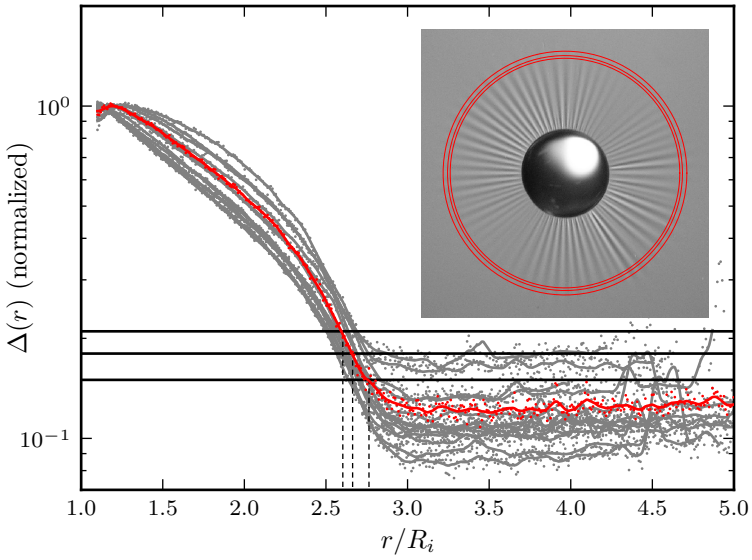

Figure S4: The standard deviation $\Delta(r)$ of the azimuthal intensity profile for 14 images of wrinkle patterns of 94 nm-thick sheets. The dots show the raw data; the solid lines show the smoothed data used for the analysis. The three horizontal lines mark the 15%, 18%, and 21% thresholds. The red curve corresponds to the image in the inset, on which are marked the lengths identified by these three thresholds.

using the limiting expression for ϕ from Eq. (39). Note that, as we have required $\tau \gg \ln \tau$ to get this result, this limit may be approached very slowly in $\tilde{\gamma}$. This explains the slow approach to the observed ratio between these two angles (Fig. 2d and S2d). Recall that these approximations are significantly better in the $\cos\vartheta_Y = 0$ case, explaining why the collapse in Fig. 2d is so much faster than that in S2d.

SI.7 Measurements and analysis

In all the results in this paper, the wrinkle length is determined from a bright-field image of the top view of the wrinkle pattern and the drop. The wrinkle length is quite well-defined in the images and a reasonable value of wrinkle length may be determined by inspection. However, one of the main results in this paper relies on a comparison of the experimentally determined wrinkle length with the prediction of the FT calculation. As a result, we preferred to use an automated analysis to extract the wrinkle length. We wish to emphasize that the precise numerical value of the wrinkle length depends (albeit weakly) on the choice of parameters used in the analysis.

Analysis procedure: The image is preconditioned with ImageJ [6] to convert it to an 8-bit grayscale image. With Matlab, azimuthal profiles of the intensity $I_r(\vartheta)$ are computed along circles of radius r centered on the drop. To remove low-frequency variations in illumination, a high-pass filter is performed on $I_r(\vartheta)$. The standard deviation $\Delta(r)$ of this profile is found at values of r from $1.1R_i$ out to a maximum radius that appears unwrinkled to the eye. The $\Delta(r)$ curve is smoothed with a 15-point triangular window. Fig. S4 shows $\Delta(r)$ plotted against r/R_i several wrinkle patterns (gray curves, with the curve corresponding to the sample image shown in red), all formed on sheets with a thickness of 94 nm.

To determine the wrinkle length, we find the radius r at which $\Delta(r)$ drops below a threshold fraction c of its maximum value. There is some variation in the noise level in each image, largely due to the fact that the illumination conditions vary depending upon the exact position of the freely floating film within the field of view of the microscope. Thus the value of c is defined not in terms of a multiple of the noise level but as a fraction of the maximum intensity. We show three choices of c ($15\%, 18\%, 21\%$ of max, black horizontal

lines in Fig. S4) chosen so that this threshold is applied close to the noise level of $\Delta(r)$. The wrinkle lengths corresponding to the 3 choices of c for the red curve are shown on the image as three red circles. For all the data in this manuscript we have used $c = 18\%$. Thus our procedure approximates the wrinkle length from below.

References

[1] B. Davidovitch *et al*, Proc. Nat. Acad. Sci. **108**, 18227 (2011).

[2] H. King, R.D. Schroll, B. Davidovitch and N. Menon, Proc. Nat. Acad. Sci. **109**, 9716 (2012).

[3] D. Vella, M. Adda-Bedia and E. Cerda, Soft Matter **6**, 5778 (2010).

[4] B. Davidovitch, R.D. Schroll, and E. Cerda, Phys. Rev. E **85**, 066115 (2012).

[5] Supplementary material to [2].

[6] ImageJ is available at http://rsbweb.nih.gov/ij/.